

Article

Li-Ion Cell Safety Monitoring Using Mechanical Parameters, Part 3: Battery Behaviour during Abusive Overcharge

Angel Kirchev * , Nicolas Guillet , Loic Lonardoni and Sébastien Dumenil

University Grenoble Alpes, CEA, Liten, Campus Ines, 50 Av. de Lac Leman, 73375 Le Bourget du Lac, France; nicolas.guillet@cea.fr (N.G.); loic.lonardoni@cea.fr (L.L.); sebastien.dumenil@cea.fr (S.D.)

* Correspondence: angel.kirchev@cea.fr

Abstract: The electrochemical and mechanical behaviour of 18,650 Li-ion cells subjected to abusive overcharge has been studied in constant current and constant voltage mode. The results from the cell deformation monitoring via a rectangular rosette strain gauges indicate an over-swelling process starting shortly after the cell voltage increases above 4.2 V. The acoustic ultrasound interrogation measurement and data treatment using clustering and mapping software, carried out in parallel, showed an abnormal evolution of the signals' power density spectral patterns, suggesting changes in the structure of the cell jellyroll induced by the overcharge reactions. The increase in cell skin temperature due to the overcharge process starts considerably later. The results suggest that the monitoring of the mechanical behaviour of cylindrical-format Li-ion cells can be used for the detection and alerting of early overcharge safety events.

Keywords: lithium ion battery; overcharge safety; strain gauge; ultrasound interrogation

1. Introduction



Citation: Kirchev, A.; Guillet, N.; Lonardoni, L.; Dumenil, S. Li-Ion Cell Safety Monitoring Using Mechanical Parameters, Part 3: Battery Behaviour during Abusive Overcharge. *Batteries* **2023**, *9*, 338. <https://doi.org/10.3390/batteries9070338>

Academic Editor: Svetlozar Dimitrov Ivanov

Received: 23 May 2023

Revised: 6 June 2023

Accepted: 14 June 2023

Published: 21 June 2023



Copyright: © 2023 by the authors. Licensee MDPI, Basel, Switzerland. This article is an open access article distributed under the terms and conditions of the Creative Commons Attribution (CC BY) license (<https://creativecommons.org/licenses/by/4.0/>).

The operation of any energy storage system comprises three basic modes: charge, discharge and open circuit stay, during which the battery cells experience a self-discharge. Both the charge and discharge processes require different control strategies indicated by the corresponding battery manufacturer in order to ensure a normal operation over the service lifetime. A failure of the discharge process control typically results in a voltage decrease below the recommended cut-off value, causing the start of undesired and often irreversible phase transformations in the active materials and current collectors of the limiting electrode (or of both electrodes when the cell design is “balanced”). Such an event does not pose a direct safety threat, except in the case when the discharge process is carried out at very high rates, substantially increasing the cell's internal temperature (e.g., during an external short-circuit). On the other hand, the management of the charge process depends strongly on the particular battery electrochemistry. When the storage system is based on an aqueous electrolyte, the charge process proceeds in parallel with the water electrolysis process at cell voltages higher than 1.23 V (the so-called “window” of thermodynamic stability of water). The competition between the principal reactions of energy storage and the water electrolysis processes becomes significant at the end of the charge of the aqueous battery cells, thus requiring the application of an extra charge quantity denoted as “overcharge”. The overcharge tolerance of aqueous batteries allows rather simple charge management of long battery strings due to the string balancing effect of the overcharge process [1]. Contrary to aqueous energy storage systems, lithium-ion (and recently sodium-ion) batteries employ aprotic electrolytes with a voltage stability window exceeding 4 V [2]. The latter allows combining a variety of electrochemical couples in cells with rather high energy density [3]. Unlike aqueous batteries, Li-ion (and sodium-ion) cells do not tolerate the overcharge well. This is due to the start of several types of undesired processes, including the electrodeposition of metallic lithium (or sodium) on the

negative electrode and different types of electrolyte solvent decomposition reactions on both electrodes [4–9]. The whole ensemble of these processes results in a rapid increase in the battery temperature and subsequent start of “overcharge type” thermal runaway and battery fire. The early detection and corresponding prevention of such events are critical for all cases of energy storage of significant volume (e.g., electric vehicles, stationary Battery Energy Storage Solutions, etc . . .). The monitoring of the mechanical behaviour of Li-ion cells is a topic of growing interest due to the potential of the corresponding methods to estimate various aspects of the battery state and battery safety [10–16]. The aim of this work is a further extension of this domain via the study of the overcharge kinetics of high-energy-density cylindrical Li-ion cells using simultaneous strain sensors and an acoustic interrogation technique as supplementary battery indicators for early signs of thermal runaway detection.

2. Experiment and Methods

The experiments carried out in this work have been part of the same measurement series presented in part 1 and part 2 of this communication [17,18]. The test subjects were lithium-ion cells from type INR18650 MJ1 (denoted as MJ1) manufactured by LG Chem (Republic of Korea), with rated voltage and capacity of 3.7 V and 3400 mAh. The cells have been equipped with rectangular rosette strain gauges “C2A-06-062LR-120” (Micro-Measurements, USA), a pair of piezoelectric transducers EPZ-20MS64W (6.4 kHz, 400 Ω) and K-type thermocouple. The overcharge experiments have been carried out at room temperature ($23 +/ - 2^{\circ}\text{C}$, air conditioned facility) inside a blast-box, using BCS-800 series battery testing equipment from Bio-Logic Science Instruments SAS (France). A picture and a short description of the experimental set-up are presented in the Supplementary Information Figures S1 and S2.

Prior to the overcharge tests, all cells underwent three “reception test” cycles at 25°C using 2 h rated discharge current (1.7 A) and 2 h-rated constant current/constant voltage (CC/CV) charge sequence with voltage limit of 4.2 V and end-of-charge current equal to 0.17 A. The cells weight and impedance at open circuit voltage and AC frequency of 1 kHz has been also checked before and after the reception tests. The resulting values have been compared with the corresponding product datasheet information in order to ensure the cells’ quality.

3. Results and Discussion

3.1. Constant Current Overcharge

The constant current overcharge tests have been carried out in the following way: a completely charged MJ1 cell equipped with a strain gauge and a pair of low-cost acoustic sensors has been discharged to a state of charge (SOC) equal to 0%, using 2 h rated current and a cut-off voltage limit of 2.5 V. After a 30 min long open circuit stay, the cell is recharged with constant current until the cell voltage exceeds a limit of 8.4 V (twice the prescribed maximum corresponding to 4.2 V). The overcharge process has been carried out with currents equal to C/10 h, C/5 h, C/2 h, C/1 h, 2 C and 3 C (C stands for the nominal cell capacity of 3400 mAh). This current range covers the most typical scenarios of EV charging, starting from overnight slow charge (C/10 h) and going up to a fast charge (2 C–3 C/6.8–10.2 A) which exceeds the recommended maximum charge current of C/1 h (3.4 A) by two or three times. Figure 1 presents the results from multi-sensing monitoring during the constant current overcharge testing campaign in terms of evolution of the cell voltage (Figure 1a), SOC (Figure 1b), skin temperature (Figure 1c), strain (Figure 1d) and received acoustic signal strength (Figure 1e). The parameter SOC has been calculated a posteriori using Ah counting [17]. The results corresponding to the charge with a current equal to C/10 h are not shown due to their similarity with the case of C/5 h rated overcharge as well as in order to get a better view of the parameters’ evolution during faster charge regimes. It can be seen that the voltage evolution during the overcharge phase (i.e., when the voltage is higher than 4.2 V) is composed of two stages. The first one consists of

a progressive increase to nearly 4.8 V, followed by a small voltage arrest ending with an instantaneous voltage increase above the limit of 8.4 V. The latter results from the activation of the CID (current interrupting device), which increases the cell resistance above $10\text{ k}\Omega$. This hypothesis has been confirmed via several teardown analyses of the positive terminal structure. The evolution of the SOC during the overcharge shows that the CID activation at low and moderate charge rates ($\text{C}/1\text{ h}$ or lower) happens when the applied extra charge exceeds 20% of the cell capacity. At higher currents, the CID activation happens sooner. The evolution of the temperature during the charge and the overcharge allows the clear distinction of two stages. During the first stage, the temperature features a plateau correlating well with the applied charge current. This indicates a relation to the Joule heating effect. The temperature starts increasing very rapidly after SOC exceeds 100%, which clearly indicates the beginning of a thermal runaway process and the occurrence of exothermic reactions inside the cells. The activation of the CID terminates the overcharge process, thus limiting the temperature maximum at 112°C at higher rates. After the termination of the overcharge, the cell temperature cools down to room temperature because the peak temperature is relatively far from the runaway point of 140°C [18]. These results show that the CID efficiently protects MJ1 cells against overcharge abuse.

The strain evolution data presented in Figure 1d show that the overcharge coincides well with a process of over-swelling of the cell (it should be mentioned that the reference point of zero deformation corresponds to SOC = 100%, and the discharge process is causing a shrinkage of the cell volume). The comparison of the evolution of the cell skin temperature with the strain data presented in Figure 1f for the case of the fastest charge rate (3 C) shows clearly that the over-swelling of the cell volume precedes the beginning of the overcharge-induced thermal runaway by a period of about 5–6 min. When the charge rate is lower, the “overcharge alert” moment of cell over-swelling appears even sooner. The latter can be seen in Figure 1g, where the temperature and the strain are compared for the case of overcharge with a current equal to $\text{C}/10\text{ h}$ (340 mA). In that case, the temperature increase is much smaller (less than 10°C) and its beginning is more than 60 min after the beginning of the over-swelling process. This result shows that a sole measurement of the temperature as an early indicator of the thermal runaway hazard induced by an overcharge abuse can be very misleading due to the small temperature increment. In contrast, the measurements of the deformation as a function of the overcharged Amp-hours does not change markedly when the applied charge current is decreased from 10.2 A to 0.34 A (i.e., more than one order of magnitude). This result demonstrates that the strain measurements can provide reliable early alert of overcharge abuse, which can be very useful in the case of an absence of individual cell voltage monitoring. It should be noted that the overcharge with different currents also strongly impacts the relaxation phase following the activation of the CID. It can be seen that in the case of high-rate overcharge (1 C–3 C), the strain decreases from nearly +1000 ppm to -500 ppm , which indicates a shrinkage equivalent to a deep discharge. In the same time, the thermal contribution to the shrinkage is between 240 and 640 ppm considering a thermal coefficient of the stain gauge being between 3 and 8 ppm/ $^\circ\text{C}$ (3 ppm/ $^\circ\text{C}$ corresponds to the high temperature measurements during the ARC tests and 8 ppm/ $^\circ\text{C}$ corresponds to the low temperature thermal cycling between -5 and 45°C , as discussed in our previous work [18]). Thus, if there is only a process of cooling down to room temperature, the strain should be in the range of +500 ppm, i.e., the cell should remain swollen, which is actually observed in all three cases of overcharge with current lower or equal to $\text{C}/2\text{ h}$. If we take into account the measurements of the pressure and the cell casing deformation, also discussed previously [18], it can be concluded that the difference in the post-overcharge deformation pattern between the high current and the low current overcharge cases is due to the opening of the cell safety valve in the first case, leading to a decrease in the gas pressure in the cell down to atmospheric pressure.

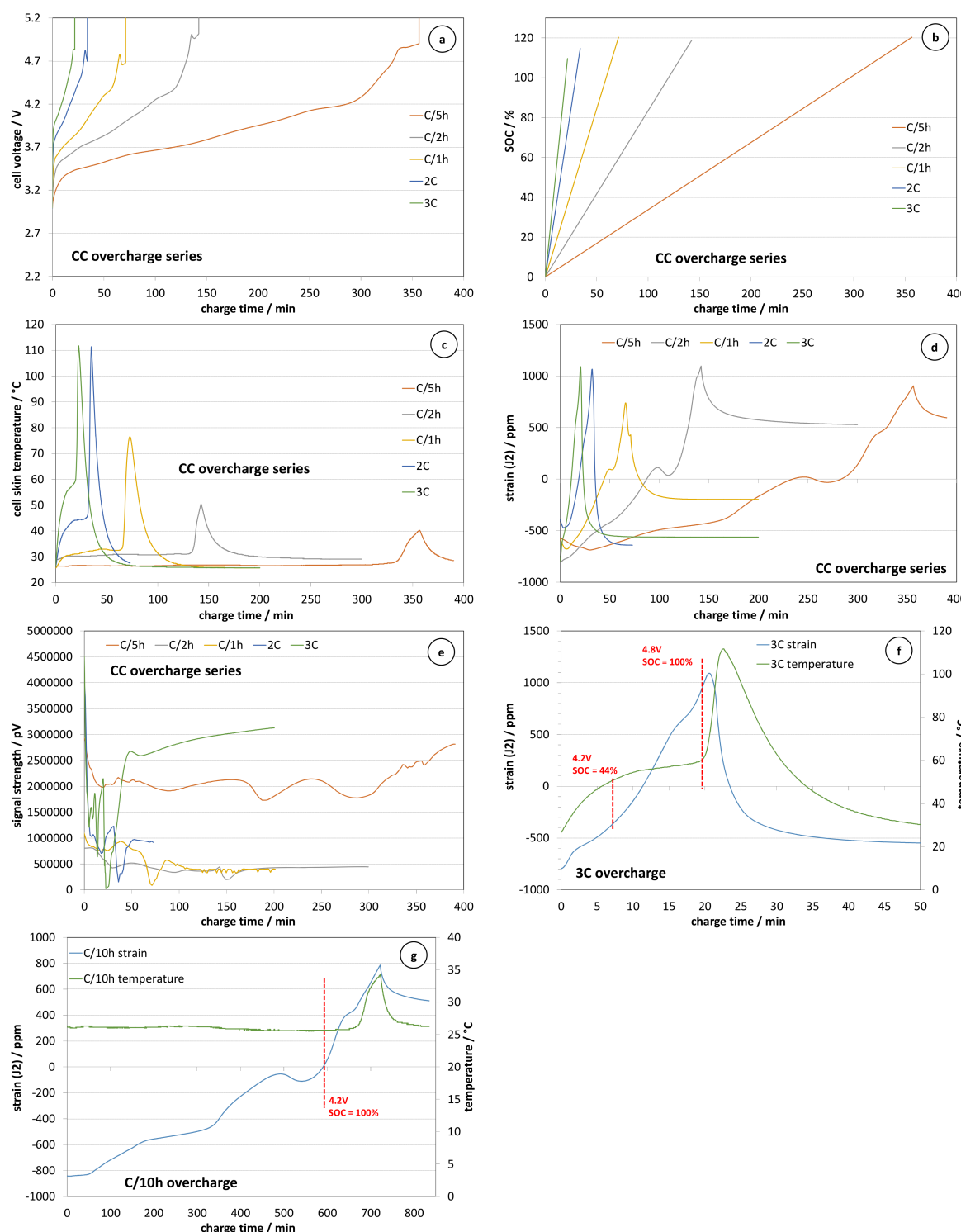


Figure 1. Evolution of the cell voltage (a), SOC (b), skin temperature (c), strain (d) and strength of the received acoustic signal transmitted through the battery (e) during overcharge tests of MJ1 cells using different currents. Zoom view of the evolution of the temperature and strain during the overcharge with 3 C and C/10 h rates (f,g).

In contrast, the cells overcharged with lower current remain sealed with high gas pressure inside. Taking into account the results for part 2 of this series [18], indicating a pressure coefficient of the deformation close to 30 ppm/bar, it can be concluded that the gas pressure inside the overcharged cells is about 15–16 bar. The latter is about twice than the

expected pressure due to the contribution of the swelling coming from the charge process. The abusive tests conducted in an Accelerating Rate Calorimeter (ARC) instrument showed that such cells (overcharged cells under pressure with activated CID) are more susceptible to thermal runaway, which makes the task of their identification particularly important [18].

Figure 1e presents the evolution of the acoustic signal strength during the ultrasound interrogation monitoring of the charge/overcharge process. At lower overcharge rates, the signal strength drops to a rather steady value, while at higher rates, it fluctuates strongly. These results can be related to a rapid increase in the internal temperature accompanied by the accumulation of gaseous products due to the overcharge reactions that reduces the propagation of ultrasound waves through the battery cell. The data suggest that further analysis using more advanced methods such as data clustering and mapping could be much more useful [17,18].

The mechanism of cell deformation during the constant current overcharge is evaluated further via a parametric analysis transforming the signals from the three gauges (J_1, J_2, J_3) of the rectangular rosette into the two-parameter plot $r(D)$. More detailed description about the interpretation of this parametric analysis can be found in the monograph of Avril [19], as well as in the supplementary information in Figure S3. The corresponding results are presented in Figure 2 for all six overcharge rates. The $r(D)$ function has been fractioned into four segments with different colours:

- “D1/r1” corresponding to $U_{cell} < 4.2$ V (safe charge process);
- “D2/r2” corresponding to $U_{cell} > 4.2$ V and $SOC < 100\%$ (electric overcharge);
- “D3/r3” corresponding to $SOC > 100\%$ until the CID activation (electrochemical overcharge);
- “D4/r4” relaxation phase after the overcharge termination.

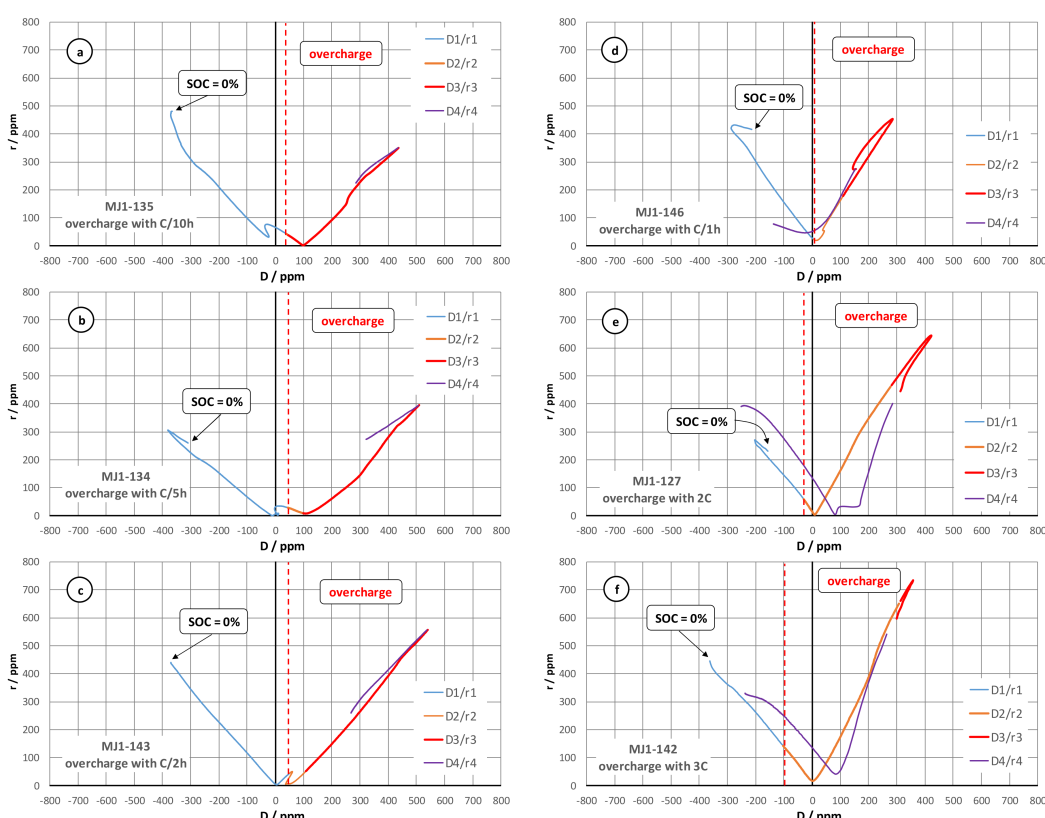


Figure 2. Parametric analysis of the cell strain behaviour during constant current charge and overcharge tests of MJ1 cells using current rates equal to $C/10$ h (a), $C/5$ h (b), $C/2$ h (c), $C/1$ h (d), $2C$ (e) and $3C$ (f).

The results from this analysis show that the increase in the charge/overcharge current does not significantly change the mechanism of the deformation process. The preferred strain orientation during the low-rate charge and the overcharge remains the increase in the cell diameter, while the increasing current (1 C–3 C) leads also to the appearance of a pulling component (increase in the cell length). The latter can be attributed to the formation of gases inside the cell jellyroll and the corresponding mechanical force of unwinding it. The $r(D)$ function allows relatively simple recognition of the overcharge abuse corresponding to points lying in the right-hand side of plot. The degree of the abusive process is nearly proportional to the growth of the right branch of the $r(D)$ function. This result can be used as a quantitative methodology for overcharge abuse risk assessment in complement with existing methods based on thermal runaway modelling [20].

3.2. Voltage-Limited Overcharge

Voltage-limited overcharge experiments have been carried out using a 2 h rated constant current/constant voltage (CC/CV) charge sequence with voltage limits of 4.6, 4.7, 4.8 and 4.9 V (each CC/CV overcharge experiment has been carried out on a “fresh” cell). The CV part of the experiment resembled the decreasing current transient observed during the regular CC/CV charge up to the voltage value of 4.8 V. The attempt to overcharge the cell with 4.9 V resulted in electrochemical behaviour similar to the case of the constant current overcharge with 1.7 A, discussed in the previous paragraph. Figure 3 presents the evolution of the cell parameters during the charge and overcharge with the other mentioned voltage limits (4.6, 4.7 and 4.8 V). The constant voltage overcharge polarization has been kept over 30 h in order to wait for delayed battery safety breach events. Due to the absence of such events, the x-axis of the plots in Figure 3 are limited to 300 min. The evolution of the cell voltage presented in Figure 3a remains repeatable during both the regular charge stage and the overcharge stage. The current transients during the constant voltage overcharge stage (Figure 1b) are very similar to those observed during the constant voltage charge with 4.2 V. The application of higher floating voltage increases the steady state value of the current exponentially (the current at 4.8 V is about 100 mA, while at 4.9 V it was in the range of 1700 mA). It should be noted that in the case of the overcharge with 4.8 V, there was a sudden drop of the current at the moment corresponding to 290 min since the beginning of the charge, which has been related to the activation of the CID. In the other two cases, the cells have been able to operate in charge/discharge mode after the tests. The evolution of SOC plotted in Figure 3c also correlates very well with the applied overcharge voltage. The maximum SOC is about 122%, which is slightly higher than the values observed in the case of constant current overcharge (120–121%).

The limitation of the overcharge voltage, limiting also the overcharge current, leads to nearly negligible changes of the cell skin temperature (Figure 3d). Such battery behaviour can be very misleading in terms of safety algorithms relying only on the measurement of the temperature, because the resulting overcharged cells are more susceptible to thermal runaway than the partially charged cells [18]. Figure 3e presents the evolution of the strain during the charge and the overcharge with a CC/CV sequence. It can be seen that despite the differences of the strain evolution at low SOC, which has been already observed during previous experiments, the deformation returns to its reference point when SOC approaches 100% in a rather repeatable manner.

The repeatability is kept further during the overcharge stage, when the cell volume swells, following closely the increase of the SOC above 100%. These results indicate a proportionality between the gas pressure build-up and the quantity of the electricity spent for the proceeding of the parasitic reactions. This suggestion has been confirmed plotting the strain data vs. the SOC considering only the points corresponding to the overcharge process ($SOC > 100\%$) until the end of the applied constant voltage overcharge (Figure 3f,g).

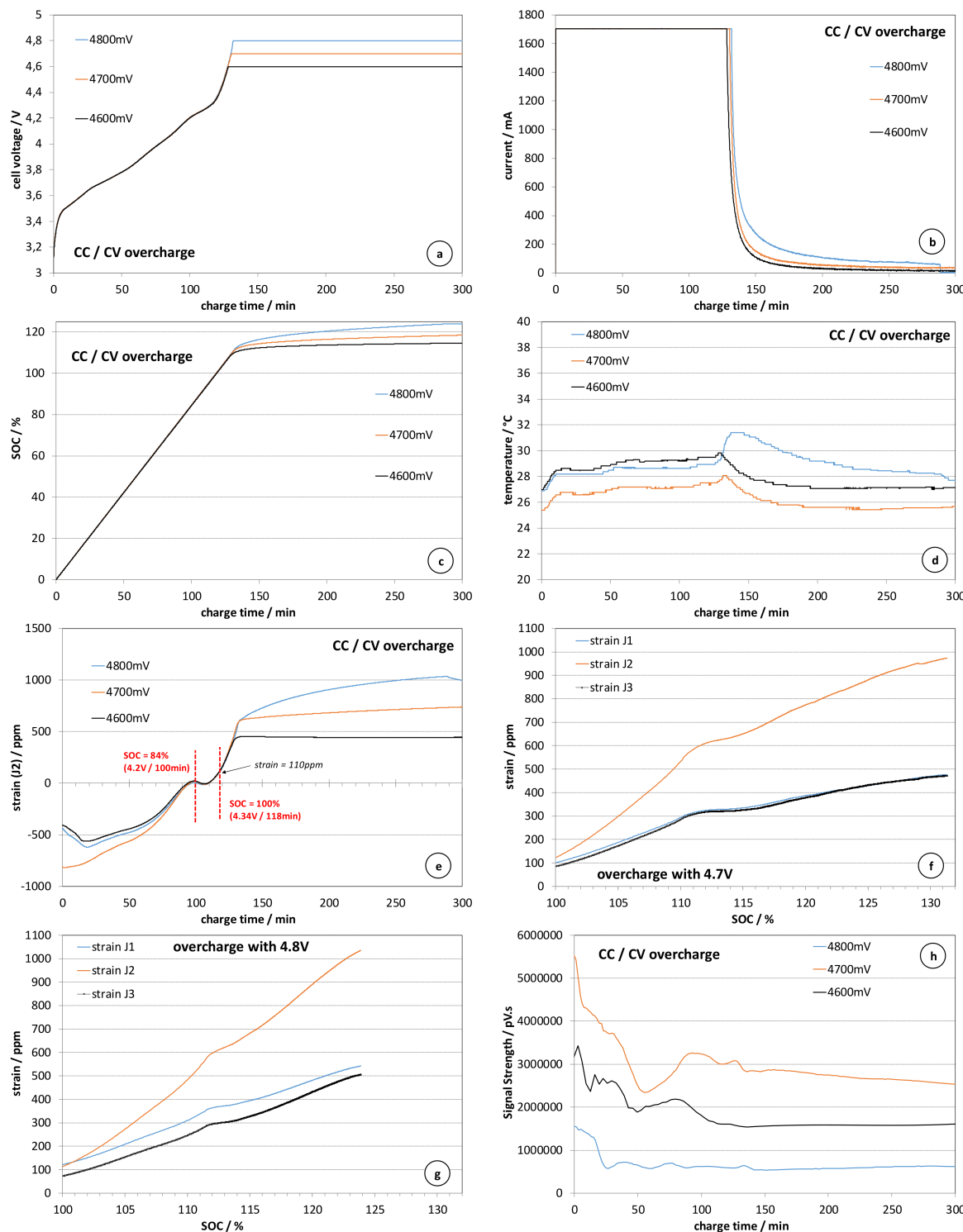


Figure 3. Evolution of the cell voltage (a), current (b), SOC (c), skin temperature (d), strain ϵ and acoustic signal strength (h) during overcharge tests of MJ1 cells using constant current/constant voltage sequence. Correlation between SOC and strain during the overcharge with 4.7 V (f) and 4.8 V (g).

The SOC vs. strain plot for the case of overcharge with 4.7 V is composed of two nearly linear segments: one up to SOC = 110–112%, and the second corresponding to SOC > 115%. In the case of the overcharge with 4.8 V, the strain increases also almost linearly with SOC again featuring two segments. The first segment is very similar to the case of the overcharge with 4.7 V; however, the slope of the second segment is higher, which indicates

faster pressure build-up inside the cell. The linear relationship between the strain and the SOC in overcharge mode ($SOC > 100\%$) can be explained combining the ideal gas law, Faraday's law and the estimated linear relationship between the strain (ε) and the fluid pressure (p_{gas}) inside the casing of the MJ1 cell, estimated as follows [18]:

$$p_{\text{gas}} = n_{\text{gas}} RT / V \quad (1)$$

$$n_{\text{gas}} = k_1 Q_{\text{ovch}} / F \quad (2)$$

$$\varepsilon = k_2 p_{\text{gas}} \quad (3)$$

where R is the molar gas constant, T is the temperature, V is the cell void volume, Q_{ovch} is the applied overcharge Amp-hours, F is Faraday's constant, n_{gas} is the number of moles of gas formed due to the overcharge reactions and k_1 and k_2 are proportionality constants. Combining the three equations, it can be seen that at a constant temperature (Figure 3d) and constant void volume inside the cell (the measured deformations correspond to negligible volume variation), the strain is proportional to the applied overcharge:

$$\varepsilon = k_2 k_1 RT (FV)^{-1} Q_{\text{ovch}} \quad (4)$$

The evolution of the strength of the acoustic signal transmitted through the battery cell presented in Figure 3h remains similar to that observed in Figure 1e for the case of overcharge with lower current. Here, the signal strength decreases to a nearly steady state value.

Figure 4 presents the results from the parametric analysis of the strain data during the constant voltage overcharge experiments. Again, the $r(D)$ function has been divided in several segments: one corresponding to the regular charge, a second corresponding to the time interval when the cell voltage is higher than 4.2 V but SOC is less than 100% and a third stage during which the cell is overcharged "electrochemically". It can be seen that the results are very similar to the data shown in Figure 2 for the case of constant current charge (especially those obtained at low-rate overcharge) except the very final stages. The predominant deformation mechanism remains the expansion of the cell diameter. In the case of overcharge with 4.8 V, the swelling continues up to a certain moment, after which there is a period of shrinkage followed by a torsion process, when the CID opens. The swelling of the other two cells continues until the end of the strain monitoring.

The overcharge tests performed on MJ1 cells using various current and voltage limits showed that the selected technology is protected rather well against overcharge abuse at the cell level. The protection device (CID) is activated by the pressure build-up, which results from electrochemical reactions forming gaseous products and heat. After activation, the electric resistance of the cells exceeds $10 \text{ k}\Omega$ and they can no longer be charged or discharged. Previous studies [18] showed that overcharged cells are stable at room temperature ($25^\circ\text{C} \pm 2^\circ\text{C}$); however, they are more susceptible to thermal abuse than cells left at $SOC = 100\%$.

Figure 5 presents the evolution of the physical properties of the acoustic signal during a normal charge–discharge cycle followed by an overcharge up to 4.8 V. The corresponding data have been subjected to the same type of clustering and mapping analysis already presented in previous publications [17,18,21]. In brief, the signal clustering and mapping tools are applied to analyse the power spectral density (PSD) of the ultrasound waves passing across the cell jellyroll diameter. It is then possible to identify different categories of PSD patterns that can be represented graphically on a 2D map and coloured depending on their position on that map. Acoustic signals presenting similar patterns (low Euclidean distance) are closely placed on the map and present the same colour. On the other hand, acoustic signals with very different patterns (large Euclidean distance) present very different colours.

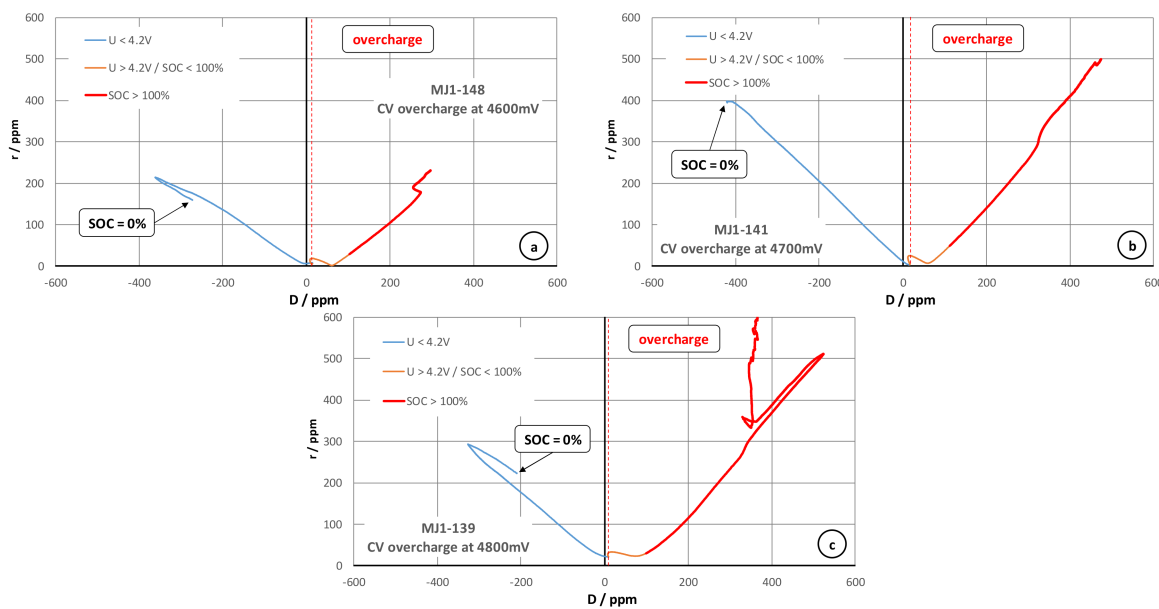


Figure 4. Parametric analysis of the cell strain behaviour during constant current/constant voltage overcharge tests of MJ1 cells using voltage limits equal to 4.6 V (a), 4.7 V (b) and 4.8 V (c).

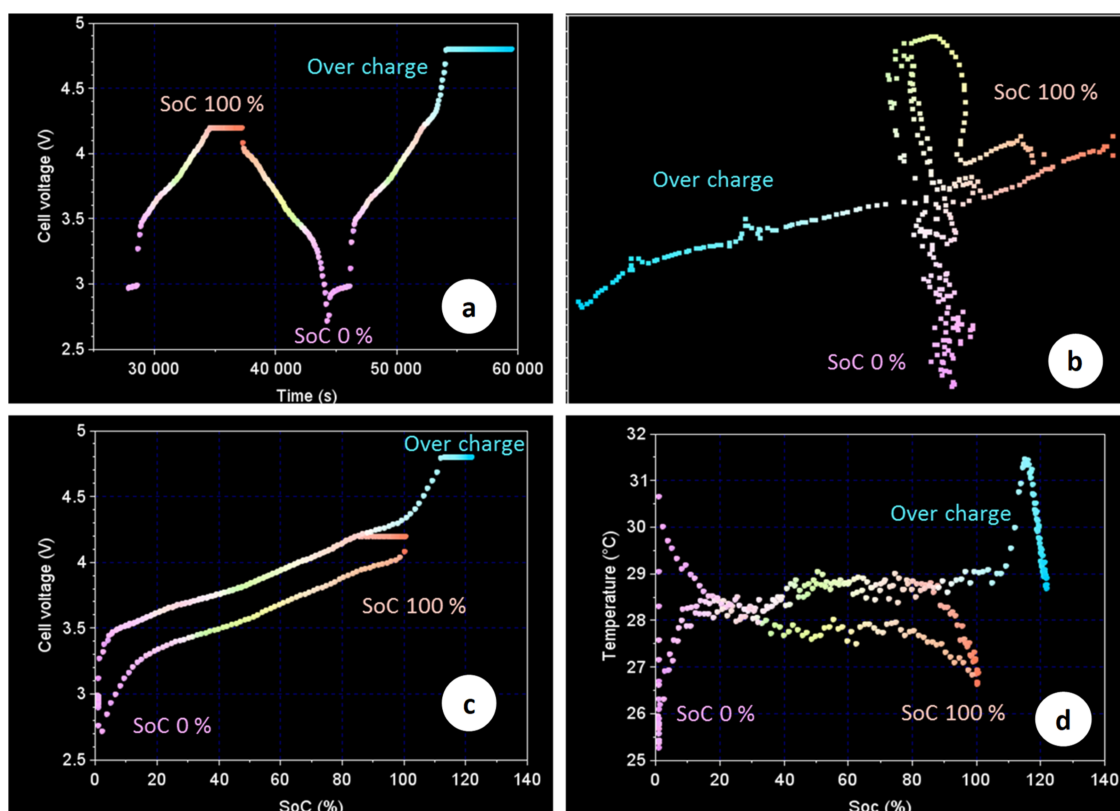


Figure 5. Clustering and mapping analysis of the acoustic ultrasound interrogation results obtained during a normal charge–discharge cycle followed by an overcharge up to 4.8 V: (a) evolution of the cell voltage versus time, (b) pseudo-3D dimensionless mapping of the acoustic signal transmitted, (c) cell voltage versus SoC and (d) cell temperature versus SoC. Colours of the dots are attributed according to the mapping positions of the PSD pattern, calculated from the Euclidean distance in between every acoustic signal transmitted through the battery cell.

Figure 5a shows that the normal charge/discharge operation proceeds with a repeatable cyclic change of the PSD patterns, which are also in good correlation with SOC (Figure 5c). It can be seen that a voltage increase above 4.2 V causes notable changes in the acoustic signal despite the fact that the amp-hour-based SOC is below 100%. The effect is particularly evident when the acoustic data are presented in a 2D space for clustering and mapping (Figure 5b). This result also coincides well with the over-swelling process observed in Figure 4. The latter starts practically when the cell voltage exceeds the value of 4.2 V. This coincidence indicates that a voltage limit of 4.2 V prevents the occurrence of a parasitic reaction with the formation of gaseous products, which increase the cell pressure (seen as increased strain) and change the cell jellyroll microstructure (e.g., through the formation of gas pockets, delamination of active materials, lithium plating, etc. . .) impeding the ultrasound passage. Figure 5d illustrates further the potential benefit of acoustic ultrasound interrogation as a method for early detection of overcharge safety breach events. The latter occur with negligible changes of the cell skin temperature, making them hardly detectable with a classic battery monitoring data set.

4. Conclusions

The monitoring of the mechanical behaviour of 18,650 Li-ion cells under abusive overcharge conditions using a rectangular rosette type of stain gauge and an acoustic ultrasound interrogation showed that both methods are capable to deliver reliable early alert information for approaching overcharge events. The strain monitoring showed that the beginning of the “electric” overcharge, defined as charge voltage exceeding the maximum limit recommended by the manufacturer, coincides well with the start of an over-swelling process. The start of the over-swelling also matches an abrupt change in the pattern of the acoustic ultrasound interrogation data, indicating changes in the cell jellyroll structure. The latter are significantly different from those observed during normal charge/discharge cycling. The overcharge proceeds further with a gradual increase in the cell voltage and cell swelling and a relatively small increase in the cell skin temperature. When the cell voltage exceeds 4.8 V, the surface temperature starts rising very rapidly, which indicates the beginning of the overcharge type of thermal runaway. The overcharge process is terminated through the activation of the CID before reaching the runaway temperature threshold of 140 °C, allowing the cells to cool down to ambient temperature and retract mechanically.

Supplementary Materials: The following supporting information can be downloaded at: <https://www.mdpi.com/article/10.3390/batteries9070338/s1>. Figure S1. Image of the strain gage “C2A-06-062LR-120”. Gage length: 1.52 mm; Overall length: 4.70 mm; Grid width: 1.27 mm; Overall width: 6.60 mm; Matrix length: 7.04 mm; Figure S2. Image of INR 18650 MJ1 cell equipped with strain gage “C2A-06-062LR-120” and coupled with piezo-electric sensors from type EPZ-20MS64W (a). Schematic representation of the ultrasound interrogation mode using a pair of piezo-electric sensors (b); Figure S3. Parametric analysis diagram for qualitative interpretation of strain measurements carried out by rectangular rosette gage and experimental r(D) patterns obtained during normal operation of MJ1 cell with different charge/discharge currents at 25 °C.

Author Contributions: Conceptualization, A.K., N.G. and S.D.; Methodology, A.K., N.G., L.L. and S.D.; Software, N.G. and L.L.; Formal analysis, A.K. and N.G.; Data curation, N.G., L.L. and S.D.; Writing—original draft, A.K.; Writing—review & editing, N.G. All authors have read and agreed to the published version of the manuscript.

Funding: This research was funded by French national program Investments for the Future (grant number: ANR-10-IEED-0014-01, INES.2S) and the European Union’s Horizon 2020 research and innovation program under the grant ‘Electric Vehicle Enhanced Range, Lifetime And Safety Through INGenious battery management’ (grant number: EVERLASTING-713771).

Conflicts of Interest: The authors declare no conflict of interest.

References

1. Berndt, D. *Maintenance-Free Batteries Based on Aqueous Electrolyte Lead-Acid, Nickel/Cadmium, Nickel/Metal Hydride: A Handbook of Battery Technology*, 3rd ed.; Research Studies Press: Boston, MA, USA, 2003.
2. Xu, K. Electrolytes and interphases in Li-ion batteries and beyond. *Chem. Rev.* **2014**, *114*, 11503–11618. [CrossRef] [PubMed]
3. Yoshio, M.; Brodd, R.; Kozawa, A. *Lithium-Ion Batteries Science and Technologies*; Springer: Berlin/Heidelberg, Germany, 2009.
4. Wen, J.; Yu, Y.; Chen, C. A review on lithium-ion batteries safety issues: Existing problems and possible solutions. *Mater. Express* **2012**, *2*, 197–212. [CrossRef]
5. Larsson, F.; Mellander, B.E. Abuse by external heating, overcharge and short circuiting of commercial lithium-ion battery cells. *J. Electrochem. Soc.* **2014**, *161*, A1611. [CrossRef]
6. Jung, R.; Metzger, M.; Maglia, F.; Stinner, C.; Gasteiger, H.A. Oxygen release and its effect on the cycling stability of LiNixMnyCozO2 (NMC) cathode materials for Li-ion batteries. *J. Electrochem. Soc.* **2017**, *164*, A1361. [CrossRef]
7. Feng, X.; Ouyang, M.; Liu, X.; Lu, L.; Xia, Y.; He, X. Thermal runaway mechanism of lithium ion battery for electric vehicles: A review. *Energy Storage Mater.* **2018**, *10*, 246–267. [CrossRef]
8. Juarez-Robles, D.; Azam, S.; Jeevarajan, J.A.; Mukherjee, P.P. Degradation-safety analytics in lithium-ion cells and modules part II. Overcharge and external short circuit scenarios. *J. Electrochem. Soc.* **2021**, *168*, 050535.
9. Juarez-Robles, D.; Vyas, A.A.; Fear, C.; Jeevarajan, J.A.; Mukerjee, P.P. Overcharge and aging analytics of Li-ion cells. *J. Electrochem. Soc.* **2020**, *167*, 090547. [CrossRef]
10. Popp, H.; Koller, M.; Jahn, M.; Bergmann, A. Mechanical methods for state determination of Lithium-ion secondary batteries: A review. *J. Energy Storage* **2020**, *32*, 101859. [CrossRef]
11. Zhu, S.; Yang, L.; Wen, J.; Feng, X.; Zhou, P.; Xie, F.; Zhou, J.; Wang, Y.N. In operando measuring circumferential internal strain of 18650 Li-ion batteries by thin film strain gauge sensors. *J. Power Sources* **2021**, *516*, 230669. [CrossRef]
12. Willenberg, L.K.; Dechent, P.; Fuchs, G.; Sauer, D.U.; Figgemeier, E. High-precision monitoring of volume change of commercial lithium-ion batteries by using strain gauges. *Sustainability* **2020**, *12*, 557. [CrossRef]
13. Daubinger, P.; Ebert, F.; Hartmann, S.; Giffin, G.A. Impact of electrochemical and mechanical interactions on lithium-ion battery performance investigated by operando dilatometry. *J. Power Sources* **2021**, *488*, 229457. [CrossRef]
14. Appleberry, M.C.; Kowalski, J.A.; Africk, S.A.; Mitchell, J.; Ferree, T.C.; Chang, V.; Parekh, V.; Xu, Z.; Ye, Z.; Whitacre, J.F.; et al. Avoiding thermal runaway in lithium-ion batteries using ultrasound detection of early failure mechanisms. *J. Power Sources* **2022**, *535*, 231423. [CrossRef]
15. Reichmann, B.; Sharif-Khodaei, Z. Ultrasonic guided waves as an indicator for the state-of-charge of Li-ion batteries. *J. Power Sources* **2023**, *576*, 233189. [CrossRef]
16. Dubarry, M.; Beck, D. Perspective on Mechanistic Modeling of Li-Ion Batteries. *Acc. Mater. Res.* **2022**, *3*, 843–853. [CrossRef]
17. Kirchev, A.; Guillet, N.; Brun-Buission, D.; Gau, V. Li-ion cell safety monitoring using mechanical parameters: Part I. Normal battery operation. *J. Electrochem. Soc.* **2022**, *169*, 010515.
18. Kirchev, A.; Guillet, N.; Lonardoni, L.; Dumenil, S.; Gau, V. Li-Ion Cell Safety Monitoring Using Mechanical Parameters: Part II. Battery Behavior during Thermal Abuse Tests. *J. Electrochem. Soc.* **2023**, *170*, 010503.
19. Avril, J. *Encyclopédie Vishay D'analyse des Contraintes Encyclopédie, NT 58C Interprétation des Mesures Extensométriques*; Vishay Micromesures: Raleigh, NC, USA, 1984.
20. Tran, M.K.; Mevawalla, A.; Aziz, A.; Panchal, S.; Xie, Y.; Fowler, M. A review of lithium-ion battery thermal runaway modeling and diagnosis approaches. *Processes* **2022**, *10*, 1192. [CrossRef]
21. Oca, L.; Guillet, N.; Tessard, R.; Iraola, U. Lithium-ion capacitor safety assessment under electrical abuse tests based on ultrasound characterization and cell opening. *J. Energy Storage* **2019**, *23*, 29–36. [CrossRef]

Disclaimer/Publisher's Note: The statements, opinions and data contained in all publications are solely those of the individual author(s) and contributor(s) and not of MDPI and/or the editor(s). MDPI and/or the editor(s) disclaim responsibility for any injury to people or property resulting from any ideas, methods, instructions or products referred to in the content.